Molecular Therapy
Nucleic Acids
Original Article

Precise template-free correction restores gene function in Tay-Sachs disease while reframing is ineffective

Joshua E. Hung,[1,2] Reid A. Brewer,[1,2,5] Lujaina Elbakr,[1,2,5] Antonio Mollica,[1,4] Georgiana Forguson,[1] Wing Suen Chan,[1] and Evgueni A. Ivakine[1,2,3]

[1]Genetics and Genome Biology Program, The Hospital for Sick Children, Toronto, ON M5G0A4, Canada; [2]Department of Physiology, University of Toronto, Toronto, ON M5S1A8, Canada; [3]Department of Molecular Genetics, University of Toronto, Toronto, ON M5S1A8, Canada; [4]Department of Biochemistry, University of Toronto, Toronto, ON M5S1A8, Canada

Tay-Sachs disease is a fatal neurodegenerative disorder caused by *HEXA* mutations inactivating the metabolic enzyme HexA. The most common mutation is c.1278insTATC, a tandem 4-bp duplication disrupting *HEXA* expression by frameshift. In an engineered cell model, we explore the use of CRISPR-Cas9 for therapeutic editing of c.1278insTATC. Within genomic microduplications, the microhomology-mediated end joining (MMEJ) pathway is favored to repair double-stranded breaks with collateral deletion of one repeat. Protospacer adjacent motif (PAM) constraints on Cas9 endonuclease activity prevented cleavage at the duplication center, the optimal position for MMEJ initiation. Rather, cleavage 1 bp from the c.1278insTATC duplication center spontaneously reconstructed the wild-type sequence at ∼14.7% frequency, with concomitant restoration of normal cellular HexA activity. As an alternative to perfect correction, short insertions or deletions were serially introduced to restore an open reading frame across a 19-bp sequence encompassing c.1278insTATC. Frame-restored variants did not recover significant HexA function, presumably due to structural incompatibility of incurred amino acid insertions. Hence, precise correction of c.1278insTATC is the only therapeutically relevant outcome achieved in this study, with MMEJ highlighted as a potential template-free CRISPR-Cas9 modality to that end.

INTRODUCTION

Tay-Sachs disease (TSD) is a neurodegenerative condition caused by recessive pathogenic mutations in the *HEXA* gene on chromosome 15. *HEXA* encodes an α-polypeptide that dimerizes with a β-polypeptide expressed by *HEXB*.[1] The folded αβ-heterodimer localizes to the lysosome as β-*N*-acetylhexosaminidase-A (HexA), the sole enzyme capable of catabolizing GM2 gangliosides.[2,3] As a membrane lipid, GM2 relies on the GM2 Activator protein, expressed by *GM2A*, to facilitate transport to the lysosome and orchestrate HexA binding.[4,5] Therefore, deleterious mutations in any of the *HEXA*, *HEXB*, and *GM2A* genes result in GM2 gangliosidosis, the spectrum of cellular pathologies and clinical symptoms resulting from neuronal accumulation of undegraded GM2.[6] Three genetically distinct forms of GM2 gangliosidosis are delineated by their locus of mutation: TSD (*HEXA*), Sandhoff disease (*HEXB*), and the AB-deficiency variant (*GM2A*).[7]

Over 200 pathogenic *HEXA* mutations have been cataloged to date, with most being *de novo* or limited to an immediate pedigree.[8–10] Indeed, TSD incidence is disproportionately driven by only a few mutations inherited within high-risk populations as established by historical genetic bottlenecks.[11] The foremost example is the c.1278insTATC mutation in Ashkenazi Jewish and Louisiana Cajun communities, which are thought to carry the allele at 1/27 frequency versus 1/300 in the general population.[11,12] This 4-bp duplication of 5′TATC at coding position 1,278 (exon 11) introduces premature stop codons via frameshift, subjecting defective mRNA to degradation and halting HexA production.[13]

Although mutation diversity and compound heterozygosity yield a wide range of phenotypes,[6,14–16] the biallelic presence of c.1278insTATC (or comparable high-pathogenicity mutations) corresponds to archetypal TSD.[4,14] Clinically, patients face the onset of neurological symptoms in infancy and a fatal prognosis by ages 4–5, with no treatments currently available.[4] The physiological threshold for HexA function is estimated to be no more than 15% of wild-type levels.[17,18] However, the difficulty of pharmacologically targeting neurons across the blood-brain barrier has hampered efforts to redress HexA enzyme deficiency and/or GM2 substrate accumulation.[4,6,7,18]

CRISPR-based genome editing excites the prospect of HexA rescue by curative correction of underlying *HEXA* mutations. While precision techniques like CRISPR prime editing show immense promise

Received 25 May 2024; accepted 21 November 2024;
https://doi.org/10.1016/j.omtn.2024.102401.

[5]These authors contributed equally

Correspondence: Evgueni A. Ivakine, Peter Gilgan Centre for Research and Learning, 686 Bay Street, Toronto, ON M5G0A4, Canada.
E-mail: zhenya.ivakine@sickkids.ca

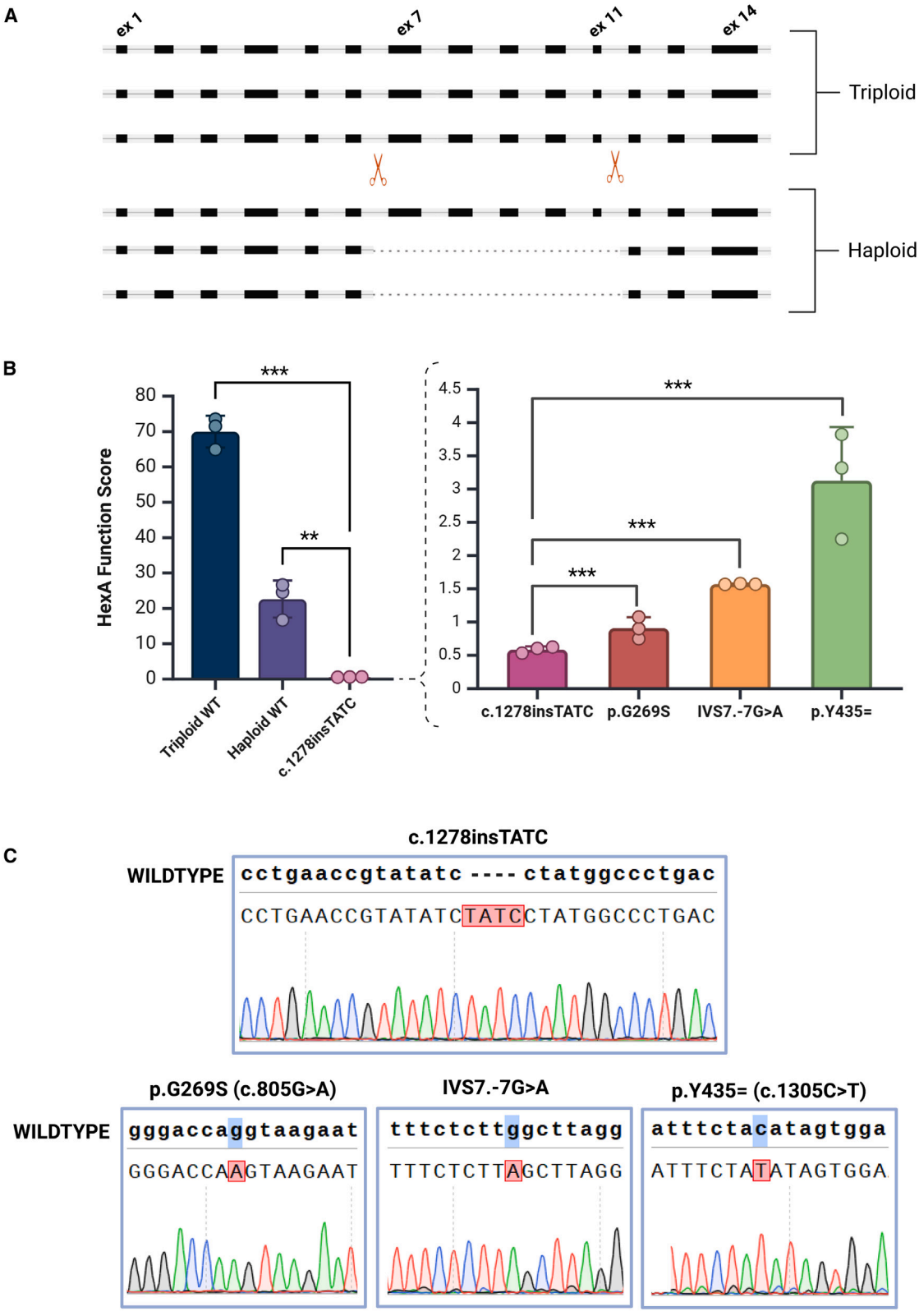

(legend on next page)

in vitro, packaging its modules into clinically applicable adeno-associated virus vectors remains a translational hurdle.[19] A simple, compact CRISPR-Cas9 system is better poised for *in vivo* testing should *in vitro* results be compelling. Accordingly, this work explores the potential of template-free CRISPR-Cas9 for therapeutic editing of c.1278insTATC in an engineered cell model. We sought precise correction of the mutation via the microhomology-mediated end joining (MMEJ) pathway; MMEJ has been outlined as a facile strategy for the predictable deletion of short duplications by targeting Cas9 at the center (i.e., duplication junction).[20] We also probed the recovery of HexA function in genomic variants of c.1278insTATC bearing short insertions or deletions (indels) that restore an mRNA open reading frame. Mutagenic CRISPR-Cas9-based frame-correction therapies have offered compelling results, notably for the *DMD* gene in Duchenne muscular dystrophy.[21–23] Should *HEXA* reframing enable expression of a physiological HexA product, frame-restoring indels from CRISPR-Cas9 targeting would offer a therapeutic alternative to wild-type correction of c.1278insTATC.

RESULTS

Haploidized HEXA locus and CRISPR prime editing for rapid modeling of TSD mutations

The transfectability and culturing resilience of the HEK293T cell line provide an effective platform for genome editing experiments. However, the *HEXA* locus of HEK293T cells is triploid by default, which enables recessive pathogenic mutations to be masked by a wild-type allele present in *trans*.[24] Hence, HexA functional deficiency in a HEK293T model of c.1278insTATC would only manifest if every allele harbored the mutation. To sidestep the burden of installing the mutation on three alleles, we first "haploidized" the *HEXA* locus—in other words, render two of the alleles null to obtain a haploid, single-allele locus (Figure 1A).

To generate the haploid locus, CRISPR-Cas9 was used to cut separately within introns 6 and 11. Excision of the interposed fragment (~4,700 bp) physically removes exons 7–11 and functionally inactivates the entire allele by frameshift. The guides targeting introns 6 and 11 were each cloned into a pU6 vector co-expressing SpCas9 and puromycin resistance. This three-in-one vector was transfected into wild-type HEK293T cells. Following puromycin selection, deletion of exons 7–11 was detected in the bulk population by allele-specific PCR alongside residual wild-type alleles (Figures S1A and S1B). After single-cell sorting and expansion of clonal lines, allele-specific PCR was repeated on clones and followed by a copy-number assay (Figures S1C and S1D) to screen for the specified configuration, two null alleles and one residual wild-type allele. A positive clone was identified, with this haploid line retaining a proportional one-third of parental triploid cell HexA activity (Figure 1B, left).

CRISPR prime editing was then used to install the c.1278insTATC duplication within the verified haploid *HEXA* HEK293T line using the PE3 modality. Summarily, the cells were transfected with the pCMV-PE2 vector expressing the nCas9 and engineered reverse transcriptase module along with pU6 vectors separately encoding the prime editing guide (peg)RNA and the secondary nicking guide (materials and methods). Installation efficiency was ~30%, and a clone positive for the c.1278insTATC allele was isolated following sorting and expansion (Figure 1C). A fluorometric assay of HexA activity (materials and methods) showed a thorough loss of activity in the c.1278insTATC line, its HexA function score two orders of magnitude lower than that of the (haploid) wild-type reference. Residual activity is attributed to basal substrate hydrolysis by other cellular glycosidases (Figure 1B, left).[1] Despite clear HexA deficiency, cellular phenotypes commonly associated with TSD, including GM2 accumulation and distended lysosomes, were not detected in HEK293T cells harboring the c.1278insTATC mutation (Figure S2).

Further cell models of patient mutations linked to milder TSD were generated using prime editing on the haploid *HEXA* locus, shown in Table 1 and Figure 1B. An identical workflow to that of the c.1278insTATC model was followed, except in the pegRNAs specifying these mutations being furnished with the TevoPreQ motif to form engineered (e)pegRNAs while forgoing a secondary nicking guide (materials and methods). Quantification of HexA function in the isolated models found higher residual HexA activities commensurate with published values (Figure 1B, right).[25–29,30] *HEXA* haploidization in HEK293T cells enables streamlined modeling of pathogenic mutations in their native genomic locus, which manifests HexA deficiency to scale but not downstream cellular pathologies.

Microhomology across Cas9 cut site in c.1278insTATC effectuates wild-type recovery

Systematic correction of microduplications by MMEJ is premised on DNA cleavage at or close to the duplication center (Figure 2A). Centered cleavage yields congruous sequences of microhomology favoring MMEJ machinery to rejoin the DNA ends. The resect-then-anneal mechanism of MMEJ is prone to collaterally deleting one copy of the microhomology,[20,32] which in the context of microduplications like c.1278insTATC reproduces the desired wild-type genotype. Junction-adjacent cleavage yields diminished and asymmetrical microhomology, but may nonetheless be amenable to MMEJ with concomitant deletion of intervening, asymmetry-causing nucleotide(s).[20]

A key constraint on MMEJ activation by Cas endonucleases is the necessary recognition of a downstream protospacer adjacent motif (PAM) to enable binding and cleavage of the sgRNA-defined DNA target. The motifs specifying the *HEXA* c.1278insTATC junction (5′CCT for sense

Figure 1. Haploidization of *HEXA* locus facilitates TSD cell models recapitulating key biochemical phenotype

(A) Schematic of CRISPR-Cas9-mediated deletion of exons 7–11 on two alleles of the triploid HEXA locus of HEK293T cells to achieve the haploid state. (B) HexA function scored in wild-type (triploid and haploid) and mutation cell lines. Error bars denote SD of mean for three biological replicates. Statistical significance from two-tailed Student's t test against c.1278insTATC denoted by $^{*}p = 0.05$, $^{**}p = 0.01$, and $^{***}p = 0.001$, respectively. (C) Sanger chromatograms for mutations modeled within haploid locus using CRISPR prime editing: c.1278insTATC, p.G269S, IVS7.-7G>A, p.Y435=.

Table 1. *HEXA* variants modeled in haploidized *HEXA* line

Mutation	Molecular defects	Associated patient phenotypes	Prime editing efficiency, %
c.1278insTATC	frameshift, mRNA nonsense-mediated decay	acute, infantile onset	30
p.G269S (c.805G>A)	missense codon[25]	acute, adult onset[25,26]	50
IVS7.-7G>A	non-canonical 3′ splice acceptor site, exon skipping[27]	chronic[28]	15
p.Y435= (c.1305C>T)	synonymous codon or alternative splicing[29]	chronic[29,31]	30

and 5′ATA for antisense) and its adjacent positions are all incompatible with the 5′NGG motifs canonically recognized by the widely used *Streptococcus pyogenes* Cas9 (SpCas9). Indeed, no Cas9 species known at the time of this work would a priori recognize the motifs needed to target c.1278insTATC for MMEJ. As such, we used an engineered SpCas9 variant with relaxed PAM requirements—SpRYCas9—to examine whether MMEJ can be a therapeutic CRISPR-Cas9 intervention for the c.1278insTATC mutation despite PAM limitations.[33]

PAM-oblivious sgRNAs specifying the junction of the c.1278insTATC duplication and the immediate upstream (−1 bp) and downstream (+1 bp) positions were screened for editing with SpRYCas9. These three positions were targeted by sense (S) and antisense (AS) strands (Figure 2B). Each sgRNA spacer was cloned into a pU6 vector expressing the spacer and scaffold along with puromycin resistance. The pU6 vector was co-transfected into c.1278insTATC HEK293T cells with a pCMV-T7 vector expressing SpRYCas9. A total of 48 h of puromycin enrichment occurred before genomic DNA was extracted and PCR amplified around the c.1278insTATC target sites for Sanger sequencing analysis.

Per Figure 2C, no edits were detected for either sgRNA targeting the junction. To verify that the lack of in-cell editing at the junction is attributable to SpRYCas9 inactivity rather than defects with the sgRNAs, a cleavage assay was performed using *in vitro* synthesized guides and purified SpRYCas9 against the target site in a PCR amplicon (Figure S3). In-cell editing was observed using the other four sgRNAs. The S +1 bp and S − 1 bp guides both resulted in spontaneous indels but not the desired duplication removal. In contrast, the antisense guides AS −1 bp and AS +1 bp elicited modest rates of precise correction alongside random indels, averaging 5.67% and 14.67%, respectively.

Within a bulk population of c.1278insTATC cells treated by the AS +1 bp guide, containing corrected wild-type cells at ∼11% frequency (Figure S4), significant recovery of HexA activity from the c.1278insTATC baseline comprises ∼13% of normal (haploid) wild-type levels (Figure 2D). Evaluated in isolation, a clonal line featuring the reconstructed wild type indicates complete restoration of wild-type HexA activity (Figure 2E).

Generation of HEXA variants from c.1278insTATC allele bearing an intact mRNA open reading frame

To assess whether non-wild-type editing outcomes could effectuate HexA rescue, we examined the effect of indels counteracting the c.1278insTATC frameshift. Given the 4-bp insertion of 5′TATC, 1-bp deletions or 2-bp insertions are plausible CRISPR-Cas9 outcomes that would restore the reading frame by net insertions of 3 bp (1 codon) and 6 bp (2 codon), respectively, compared to wild-type *HEXA*. Proactively testing the functional outcome of reframing across the c.1278insTATC mutation and adjacent sequences can inform future approaches to therapeutic editing interventions for this mutation. We selected a 19-bp window that spans plausible boundaries for intervention, starting upstream of the mutation from the 5′ATA codon encoding Ile425 (preserving preceding codons for active site residues Asn423 and Arg424)[34] and ending at the induced premature stop codon 5′TGA (Figure 3A).

In total, 17 reframed genomic variants were established as cell lines (Figure 3B). Variants 1–15 represent all unique single base pair deletions across the 19-bp window, with consecutive nucleotides resulting in four genetically redundant variants. Prime editing was used to derive each 1-bp deletion from the c.1278insTATC allele, except for variant 9 (deletion of C) being isolated as a stochastic CRISPR-Cas9 product thanks to a 5′NGG PAM at the relevant position. Two spacer sequences were employed for epegRNAs across the 19-bp sequence (Table S2); the reverse transcriptase (RT) template was serially modified to encode each deletion and configured with a 10-bp primer binding (PB) site. The epegRNAs were cloned into a pU6 vector and individually co-transfected with the PE2 construct into c.1278insTATC cells. Editing was efficient, generally exceeding 40% for each epegRNA. Edited populations were pooled into a heterogeneous mixture for single-cell sorting, and expanded clones were screened until all 15 variants were isolated. The two additional variants (16 and 17) each carry a random 2-bp insertion between the 7th and 8th nucleotides of our selected window; these two variants were isolated from the editing of c.1278insTATC cells by the AS +1 bp guide, as previously described.

The 17 genetically distinct variants translate to 12 unique polypeptides, assuming normal splicing and mRNA processing. The amino acid change(s) entailed by each variant are shown in Figure 3B. At minimum, each reframed variant carries an insertion (italicized residue), while some variants also impose substitutions (underlined residues) through vestigial c.1278insTATC insertion nucleotides. Mapping these polypeptide changes against wild type (Figure 3A) reveals that collectively across the 17 variants, the wild-type residues subject to substitution are Ile425, Ser426, Tyr427, and Gly428, while Arg424 through Pro429 adjoin the various inserted residues (via C and/or N terminus).

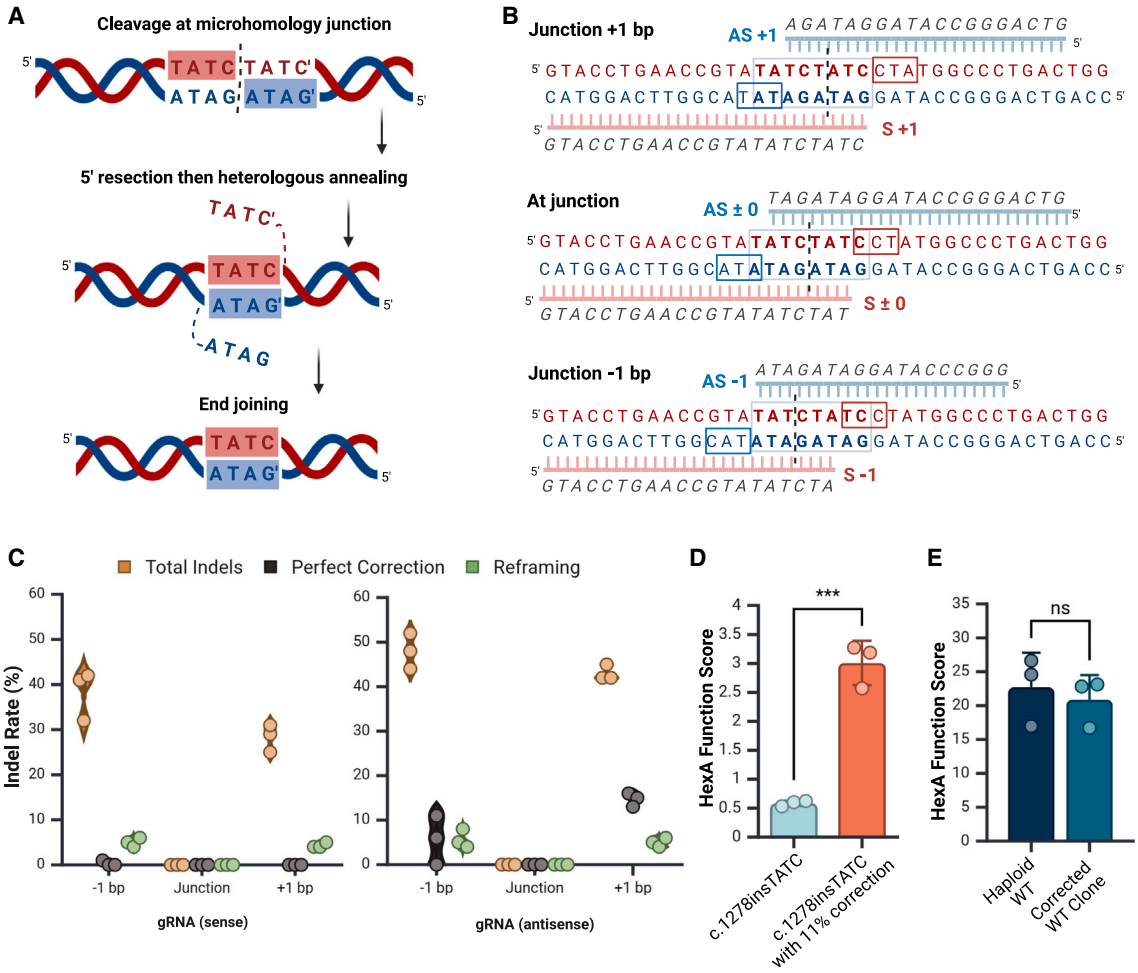

Figure 2. MMEJ-mediated correction of c.1278insTATC allele by SpRYCas9 targeting

(A) Schematic for precise correction of c.1278insTATC to wild type via MMEJ. Reannealing of heterologous 5′ TATC and 5′ ATAG sequences (highlighted) following double-stranded break. The resected 5′ TATC and 5′ ATAG copies (not highlighted) are deleted prior to re-ligation. (B) Sense and antisense sgRNA sequences tested for the duplication junction and its two adjacent positions. Boxed motif indicates the notional PAMs (blue for sense, red for antisense) pertaining to each target position. (C) Indel profile generated by sgRNA using SpRYCas9 with 48 h of antibiotic selection (gold, total; black, wild type; green, non-corrective, frame-restoring). (D) Significant recovery of HexA function in c.1278insTATC population heterogeneously edited by AS +1 bp sgRNA containing wild-type cells at 11% frequency. SD of mean shown across three independent experiments. Two-tailed, unpaired t test performed with significance set at ns = $p > 0.05$; *** = $p < 0.001$. (E) HexA activity in perfectly corrected clone isolated from AS +1 bp sgRNA editing is on par with wild-type reference.

Reframed HEXA variants entailing amino acid changes do not recover significant HexA function

HexA activity of whole-cell lysates was scored for the 17 reframed *HEXA* variants using the fluorometric assay as before (Figure 4A). Apparent increases in HexA activity from the c.1278insTATC baseline were suggested by a significant Welch's one-way ANOVA ($p = 0.001$). However, the post hoc analysis returned statistical significance only for variant 3 ($p = 0.006$), revealing no true restoration of HexA function in the other 16 reframed variants.

As indicated above, Arg424 through Pro429 are the six residues disrupted by substitution and/or insertions to reframe the c.1278insTATC allele. To provide context, we identified the location of these affected residues within the normal structure of HexA using Mol* three-dimensional (3D) visualization; Figure 4B shows the crystal structure of the HexA heterodimer with Arg424 through Pro429 called out as dark purple ball-and-stick residues. Figure 4C is an enlarged view of residues highlighted in Figure 4B. As depicted, Arg424 through Pro429 reside along an α and β subunit interface. Notably, these perturbed residues are also in close proximity to residues comprising the active site within the α subunit (ball-and-stick residues colored in blue) as elucidated by Lemieux et al. in their crystallographic studies of HexA.[34] Two of the residues perturbed in our reframing experiments, Arg424 and Tyr427, are proposed by Lemieux et al. to participate directly in catalysis by mediating active site binding of GM2 and coordinating β chain residues, respectively.[34]

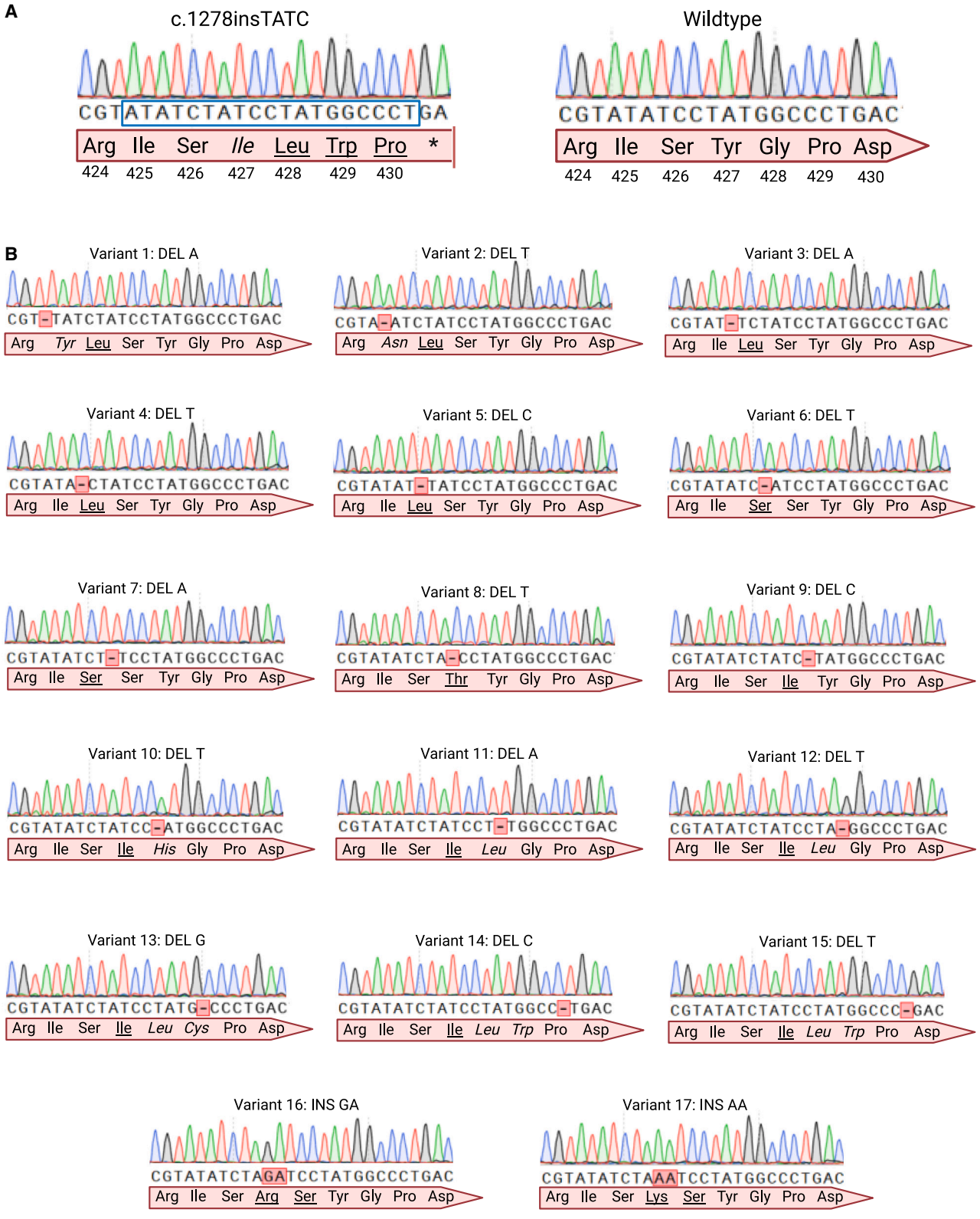

(legend on next page)

DISCUSSION

The cellular models generated for this study exemplify the utility of prime editing and locus haploidization techniques to recapitulate *HEXA* mutations whose functional significance can be discretely evaluated. The four modeled mutations also usefully represent a gradient of HexA activity levels and clinical phenotypes that help calibrate our interpretation of the therapeutic significance of any HexA functional recovery resulting from genetic editing. In particular, the p.Y435= (c.1305C>T) variant corresponds to an atypically mild phenotype[31]; this C-to-T substitution is putatively synonymous but empirically found to engender aberrant splicing.[29] In our assay, p.Y435= cells register ∼13.8% of wild-type HexA activity, just short of the 15% physiological threshold.

In our sample of 17 indels reframing the c.1278insTATC allele, only variant 3 exhibits statistically significant functional recovery, but at ∼5.47% of wild type, recovery is short of physiological levels. Benchmarked against the p.G269S and IVS7.-7G>A *HEXA* variants, for which we observed ∼4.02% and ∼6.95% of wild-type activity, respectively, the magnitude of recovery in a homogeneous population of variant 3 could plausibly reduce phenotype severity vis-à-vis the c.1278insTATC baseline. However, we expect any such effect to be therapeutically insignificant in a heterogeneously edited population. Thus, we find no actionable therapeutic potential in *HEXA* reframing across our 19-bp window encompassing the full c.1278insTATC duplication sequence.

HexA enzyme function is predicated on the assembly of the α-polypeptide (*HEXA*) and β-polypeptide (*HEXB*) subunits.[34] Degradation of truncated *HEXA* mRNA produced by the c.1278insTATC allele preempts the assembly of HexA.[13,29] In theory, frame-restoring indels could circumvent mRNA degradation and enable expression of an α-polypeptide, albeit mutant, which may heterodimerize into a catalytically active product. However, our present study finds no meaningful recovery of catalytic activity following reframing.

Since the α-polypeptide residue insertions/substitutions induced by frame-restoring indels reside at a key inter-subunit region of HexA, we speculate that those amino acid changes may compromise the functional/structural integrity of the nearby active site cavity and/or destabilize critical contacts with the β-polypeptide. Unstable HexA structures are typically retained and degraded in the endoplasmic reticulum rather than processed for lysosomal uptake.[30,35] While the precise consequences of reframing on HexA folding and active site architecture are beyond the scope of this work, the observation of HexA functional deficiency despite reframed mRNA suggests delicate functional genomics at play. As a compact catalytic protein of ∼54 kDa, the poor tolerance of HexA for modest amino acid alterations needed to reimpose an mRNA open reading frame hampers the therapeutic feasibility of reframing the c.1278insTATC allele. In contrast, reframing strategies for genes producing larger, structural proteins such as *COL7A1* (COL7A),[36] *NEB* (nebulin),[37] and *DMD* (dystrophin) show considerable promise, including the skipping of select whole exons.[38–40]

One distinctive reframing outcome absent in this study is non-corrective 4-bp deletions on the c.1278insTATC allele. While not restoring the wild-type genotype, such deletions would avoid amino acid insertions and limit perturbation to residue substitutions. Substitutions alone within HexA may be more innocuous and yield considerable hypomorphic function. Furthermore, certain tetranucleotide deletions around the c.1278insTATC duplication would reframe the transcript to be synonymous with codons synonymous with those of wild-type HexA. We raise this possibility that physiological HexA function may not absolutely require the wild-type genotype, but because 4-bp deletions are rare as stochastic indels, it is beyond the template-free CRISPR-Cas9 premise of this work.

Since the sensitive functional genomics of *HEXA* dismiss therapeutic prospects for spontaneous, untemplated reading frame correction, restoring the wild-type sequence to c.1278insTATC remains the clearest path to HexA rescue. To that end, our SpRYCas9 editing experiments offer a basic blueprint to induce MMEJ for precise correction. The most effective guide we tested—antisense cutting +1 bp from the center—produced the wild-type sequence at a mean frequency of ∼14.7% of all sequencing reads in the bulk population, representing approximately one-third of all indels. The notable corollary is MMEJ being outcompeted as evidenced by the ∼2:1 prevalence of random indels (including ineffective reframe events) characteristic of the non-homologous end joining (NHEJ) pathway.

The three positions targeted within c.1278insTATC lack the canonical 5′NGG PAM of wild-type SpCas9. While the PAM-promiscuous SpRYCas9 successfully cut 1 bp from the c.1278insTATC junction, our inability to cleave exactly at the junction is a major limitation that is likely responsible for the relative sluggishness of MMEJ vis-à-vis NHEJ. When targeting the PAM-supported junctions of *LMDG2* and *HSP1* microduplications, Iyer et al. report repair profiles dominated by MMEJ, with precise correction comprising 70%–80% of all indels.[20] Interestingly, targeting 2 and 4 bp away from the junction of the 16-bp *HSP1* microduplication was still effective, with 50%–60% of indels being precise correction.[20] We interpret cuts positioned away from the junction to be more detrimental to MMEJ in our 4-bp c.1278insTATC *HEXA* microduplication compared to a 16-bp microduplication with more extensive microhomology at its disposal. All this said, the lack of favorable PAM conditions and sub-optimal activation of MMEJ are translational concerns for the correction of c.1278insTATC via CRISPR-Cas9. Nonetheless, this study validates

Figure 3. Derivation of *HEXA*-reframed variants from c.1278insTATC allele

(A) Region selected for frame-restoring mutagenesis along the c.1278insTATC allele shown in rectangle: spanning A of ATA codon (Ile425) through T of TGA codon (premature stop). Wild-type sequence and polypeptide shown for reference on the right. (B) Sanger chromatograms of reframed variants with operative indel. Corresponding polypeptide residues presented below, with italicized and underlined residues respectively indicating insertions and substitutions compared to wild type.

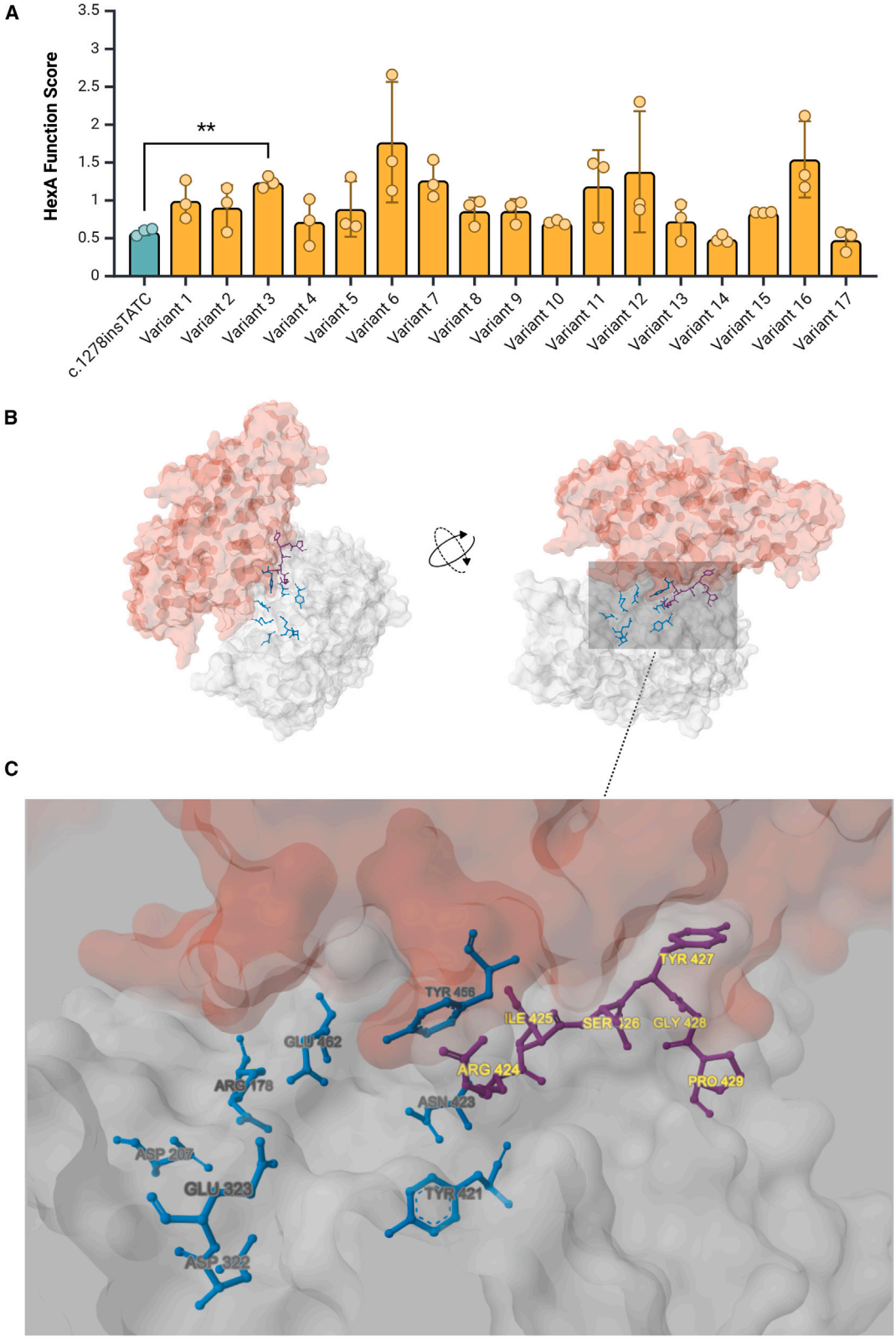

(legend on next page)

the general framework of Cas9-activated MMEJ for facile, template-independent correction of the c.1278insTATC allele. Eventually, cleavage at the c.1278insTATC junction for more robust MMEJ activity may become possible through newly isolated/engineered PAM-compatible Cas enzymes.

Toward a prospective clinical MMEJ-based therapy for c.1278insTATC, several other translational parameters remain unclarified by our HEK293T cell model. First, the vigor of MMEJ against NHEJ in the post-mitotic environment of neurons is unclear.[41,42] Second, the lack of phenotypes like GM2 accumulation or lysosomal distension in our HEK293T model also precludes assessing how mutation correction may correspond to reversal of disease markers and cellular pathologies. The lack of the lipid-related phenotype HexA-deficient HEK293T cells may be due to fundamental differences in GM2 metabolism compared to neural tissue. Third, the *in vivo* correction threshold to restore physiological HexA function in the CNS has not been elucidated either. In this study, corrected wild-type cells at 11% frequency in a treated c.1278insTATC population (Figure S2) returned ∼13.3% of wild-type HexA activity, which may hint at a near 1-to-1 linearity between genetic correction and functional recovery. While this rate of in-cell editing approaches the benchmark 15% of wild-type function, it is the result of enrichment; whether such levels of correction are achievable *in vivo* is uncertain. *In vivo* correction thresholds could additionally be nuanced by the spatial distribution of corrected cells in tissue and cross-correction dynamics between organ systems.[6,43] Ultimately, comprehensive *in vivo* models are needed to determine whether the MMEJ strategy for c.1278insTATC correction is clinically feasible.[44]

Altogether, we find no therapeutic capacity in reading frame restoration on c.1278insTATC whereby amino acid changes are incurred in HexA. In our template-free CRISPR-Cas9 editing context, precise MMEJ-mediated correction is the only therapeutically relevant outcome, presented here as a proof-of-principle pending *in vivo* study.

MATERIALS AND METHODS

CRISPR genome editing constructs

General plasmid preparation

Plasmid-based delivery of CRISPR constructs to HEK293T cells was used. Competent TOP10 *Escherichia coli* cells (prepared in-house by calcium chloride) were transformed with plasmids by heat shock, after which bacterial cells were plated and grown overnight at 37°C on Luria broth (LB) agar plates with carbenicillin (50 μg/mL) per plasmid-conferred resistance. Subsequent colonies were inoculated in LB with carbenicillin and further cultured for 12–15 h. Plasmid DNA was isolated using the QIAprep Spin Miniprep kit (Qiagen).

CRISPR-Cas9 sgRNA design and cloning

Single-guide RNA (sgRNA) design occurred across two CRISPR-Cas9 editing contexts. The first was generation of the haploid *HEXA* locus in HEK293T cells, targeting introns 6 and 11 for the deletion of exons 7–11, prior to mutation modeling. The CHOPCHOP web tool (https://chopchop.cbu.uib.no/) predicted target sequences within introns 6 and 11, engendering high SpCas9 activity.[45] Second, for PAM-ignorant editing experiments on 1278insTATC using SpRYCas9, target positions were pre-fixed. Hence, spacers were simply taken as the sequence ending 3 bp upstream of the intended cut site and starting 17–22 nt upstream to feature G at the 5′ end of the spacer to promote expression within plasmids. A 5′ G was prepended to all sgRNA spacer sequences without an endogenous G. Spacer sequences are listed in Table S1. Spacer sequences and complements were synthesized as oligonucleotides by Integrated DNA Technologies (IDT) with 5′CACC and 5′AAAC overhangs, respectively, to facilitate restriction enzyme cloning into the linearized plasmid containing the Cas9 scaffold sequence. Spacers and their complements were annealed with a Tris-EDTA buffer and then were ligated into the compatible sticky-ended plasmid backbone using T4 DNA ligase (Thermo Fisher Scientific). The sgRNA spacer sequences targeting introns 6 and 11 for *HEXA* haploidization were cloned into the SpCas9(BB)-2A-Puro (PX459) version 2.0 vector containing the sgRNA scaffold plus SpCas9 and puromycin resistance cassettes provided by the Zhang lab (https://www.addgene.org/62988/). This vector was linearized by BbsI (New England Biolabs [NEB]) digestion to generate the compatible overhangs for directional assembly with the spacer sequences. Spacers sequences for c.1278insTATC editing were cloned into BPK1520-puroR shared by the Cohn lab (https://www.addgene.org/173901/). Compatible sticky-end ligation sites were generated by BsmBI (NEB) digestion. BPK1520-puroR co-expresses puromycin resistance with the spacer and scaffold. The SpRYCas9 was expressed on a separate vector, pCMV-T7-SpRY-P2A-EGFP (RTW4830), provided by the Kleinstiver lab (https://www.addgene.org/139989/).

In vitro *cleavage assay*

In vitro cleavage was performed to validate the antisense and sense guides targeting the c.1278insTATC duplication junction. Purified SpRYCas9 (NEB) was complexed with synthesized sgRNAs and a PCR amplicon containing the target site as the substrate. PCR primers were the same as those used to amplify across the duplication for sequencing (Table S3). sgRNA synthesis was carried out using the MEGAshortscript T7 Transcription Kit (Thermo Fisher

Figure 4. Marginal HexA function rescued by frame-restoring indels disrupting amino acid near active site

(A) HexA function scores for reframed variants derived from c.1278insTATC HEK293T cell line through 1-bp deletions or 2-bp insertions. Error bars indicate SDs across three biological replicates. Omnibus significance indicated by one-way Welch's ANOVA (p = 0.001), with Games-Howell multiple comparisons test against c.1278insTATC baseline detecting significance for variant 3 (p = 0.006). (B) Structure of wild-type HexA (β subunit in red, α subunit in gray) highlighting residues affected by reframing at arbitrarily selected poses (right and left sides). Perturbed α subunit amino acids Arg424 through Pro429 shown as dark purple ball-and-stick residues. Nearby active site residues within α subunit shown as sky blue ball-and-stick residues. (C) Magnified view of right-side pose in (B) with residues labeled.

Scientific) and purification was done by sodium acetate-ethanol precipitation. Custom synthetic DNA oligonucleotides containing a T7 promoter in tandem with the desired sgRNA sequence (IDT) served as transcription templates per protocol shared by Varshney et al.[46] Cas9, sgRNA, and substrate DNA were used at 90, 90, and 9 nM, respectively, in a 1-h reaction at 37°C terminated by 15 min of Proteinase K treatment. Products were analyzed by running the reaction mixture on a 2% agarose gel. Cleavage efficiency was quantified by relative band intensities using Image Lab (Bio-Rad).

epegRNA design and cloning

Prime editing experiments employed the PE2 construct consisting of a pegRNA and a nickase Cas9 (nCas9), which nicks the DNA at the target site and is fused to an engineered RT module.[44] The pegRNA features the spacer and scaffold of a traditional sgRNA plus an extension off the 3′ end comprising two distinct segments: the RT template and the PB site. The RT template sequence contains the desired edit to be reverse transcribed into the genome by the RT module, while the PB site is made complementary to the 3′ flap of the DNA strand nicked by the nCas9; the resulting duplex thus "primes" the reverse transcription reaction off the free 3′ end.[44] If the newly edited 3′ flap successfully re-ligates into the nicked strand and transmits the edit to the unnicked, unedited strand during mismatch reconciliation, then the edit is stably incorporation into the genome.[47] PE3 permutations of prime editing target the unedited strand with a secondary nicking guide, which is intended to direct mismatch repair in favor of the newly edited strand. In this study, pegRNA spacer sequences were identified through 5′NGG PAMs in the vicinity of target sites. Final pegRNA designs were informed by RGenome web tool suggestions on RT template and PB site configurations (http://www.rgenome.net/pe-designer/).[48] Appendage of the TevoPreQ motif (5′cgcggttctatctagttacgcgttaaaccaactagaa) on the 3′ terminus of the PB site was used to form the epegRNA modality for enhanced structural stability vis-à-vis the standard pegRNA.[49] All pegRNA sequences are provided in Table S2. epegRNA sequences were cloned into the pU6-pegRNA-GG-acceptor from the Liu lab (https://www.addgene.org/132777/) and co-transfected with the pCMV-PE2 vector expressing the PE2 construct, which consists of SpCas9 nickase (H840A) and engineered Moloney murine leukemia virus RT (https://www.addgene.org/132775/). The pU6 vector was linearized by PCR (forward: 5′atcacaaaaatcgacgctcaag; reverse: 5′ggtgtttcgtcc tttccaca) using CloneAmp HiFi PCR Premix (Takara) for 32 cycles (10-s denaturation at 98°C, 10-s elongation at 60°C, and 10-s extension at 72°C). epegRNA sequences were synthesized by IDT as DNA "eblock" fragments bearing 20–30 nt of homology to both ends of the linearized backbone. Homology-based assembly was done using NEBuilder HiFi DNA Assembly Master Mix (NEB) through a 1-h incubation at 50°C.

Cell culture and harvesting

General conditions and procedures

HEK293T cells were sourced from American Type Culture Collection and cultured at 37°C and 5% CO_2. Standard culturing media was DMEM supplemented with heat-inactivated fetal bovine serum (FBS) and penicillin/streptomycin cocktail (Wisent) at 10% and 1% v/v, respectively. Adhered cells were detached using 0.25% trypsin with 0.53 mM EDTA in Hank's balanced salt solution (Wisent). The cell suspension concentration was found using a CountessTM 2 FL Automated Cell Counter (Thermo Fisher Scientific). For cryopreservation, freezing media consisted of a 1:3:6 volumetric ratio of DMSO:FBS:DMEM. Samples were cooled in a Mr. Frosty chamber (Nalgene) before transferring to liquid nitrogen storage.

Transfection

Transfection was done with Lipofectamine3000 (Thermo Fisher Scientific) per the manufacturer's guidelines. For classic transfection, cells were seeded and cultured overnight for ∼80% confluency at the time of transfection, while reverse transfections added cells at ∼80% confluency following on-plate transfection complex preparation. Total DNA, 1500 and 500 ng, were used for transfection in 12-well and 24-well plates, respectively. A 1:1 mass ratio of guide- and Cas protein-expressing plasmids was generally used for editing experiments. Puromycin selection was done at 2 μg/mL starting 24 h after transfection for 48–72 h, with antibiotic media refreshed every 24 h.

Cell sorting

Cells were sorted into 96-well plates and clonally expanded in supplemented DMEM. Sorting by flow cytometry was performed at the SickKids-UHN Flow Cytometry Facility (Toronto, Ontario, Canada) on a MoFloXDP sorter (Beckman Coulter); cells were suspended at 10^6 cells/mL in fluorescence-activated cell sorting buffer (PBS sans Ca^{2+} and Mg^{2+}, 2% v/v FBS, 2.5 mM EDTA), filtered by a 40-μm strainer and stained with 0.1% v/v propidium iodide in polypropylene tubes. Alternatively, manual sorting was performed by limiting dilution. Per 96-well plate, cells were serially diluted to ∼45 cells in 10 mL media; 100 μL of this diluted cell suspension was pipetted into each well for an average seeding density slightly under 0.5 cells/well. Colonies were expanded for 14 days or until ready for analysis.

Protein isolation

Extraction from cell pellets began with a PBS (137 mM NaCl, 2.7 mM KCl, 10 mM Na_2HPO_4, 1.8 mM KH_2PO_4 at pH 7.4) wash, then a 30-min incubation on ice with lysis buffer (1% v/v Triton X-100, 50 mM Tris-HCl at pH 7.4, 150 mM NaCl, 5 mM EDTA, supplemented with 0.25 mg/mL human serum albumin [Thermo Fisher Scientific] to support the miscibility of HexA). Lysate was centrifuged at 20,000 × *g* at 4°C for 15 min, the pelleted debris discarded, and protein collected as the supernatant. Protein concentration was determined using the Pierce BCA Protein Assay Kit (Thermo Fisher Scientific).

DNA extraction

DNA extraction for crude-lysis PCR applications used DirectPCR Cell reagent (Viagen), while genomic DNA extraction was performed with the Blood & Tissue Kit (Qiagen). DNA concentration was measured by nanodrop spectrophotometer.

Molecular and biochemical analysis

PCR

PCR products for analysis (electrophoresis, Sanger sequencing) were amplified with DreamTaq PCR Master Mix (2×) (Thermo Fisher Scientific) or Q5 High-Fidelity 2× Master Mix (NEB). Primer sequences are listed in Table S3.

Gel electrophoresis

Agarose gels, 0.8%–2% w/v, were used for the electrophoresis of DNA fragments. Agarose gels were cast with TAE buffer (40 mM Tris, 20 mM acetic acid, 1 mM EDTA, at pH 8.3) and ethidium bromide added at 0.6 μg/mL. Gel visualization took place on a Bio-Rad GelDoc instrument and Image Lab software.

Sanger sequencing

Sanger sequencing of purified PCR products or plasmids was either performed by The Centre of Applied Genomics (TCAG; Toronto, Ontario, Canada) or in-house on an Applied Biosystems SeqStudio Genetic Analyser with BigDye Terminator version 3.1 Cycle Sequencing and xTerminator Purification kits (Thermo Fisher Scientific) following the manufacturers' protocols. Primers used for sequencing are shown in Table S3.

Deconvolution of CRISPR edits

Genetic heterogeneity in cell populations arising from CRISPR-Cas9 editing was analyzed with the Inference of CRISPR Edits (ICE) web tool from Synthego (https://ice.synthego.com).[50] ICE traces indel editing events and provides their estimated frequencies within a population. For single-nucleotide substitutions, estimates were based on thr proportion of mutant to wild-type base calls given by Sanger sequencing.

Digital PCR

Digital PCR-based copy-number analysis of *HEXA* in HEK293T was performed by TCAG. The assay probe targeted intron 10 to confirm the haploidization of *HEXA* via a single residual copy of exons 7–11 without translocation of excised copies to other genome sites. The RNase P locus served as the reference.

Fluorometric HexA assay

HexA activity within whole-cell lysates was assayed using 4-methylumbelliferyl 6-sulfo-2-acetamido-2-deoxy-β-D-glucopyranoside (MUGS), a synthetic substrate that releases the 4-Methylumbelliferone (MU) fluorophore (excitation at 360 nm, emission at 450 nm) upon hydrolysis.[30] The anionic sulfated moiety of MUGS mimics the negatively charged NANA residue on the native HexA substrate, GM2, making MUGS a highly specific proxy.[3] For each sample, 5 μg lysate was diluted in citrate phosphate buffer (100 mM citric acid, 200 mM dibasic sodium phosphate, prepared at pH 4.5) to a working volume of 25 μL. The 25 μL lysate was then mixed with 25 μL MUGS substrate (Toronto Research Chemicals), prepared as a 3.2-mM solution in citrate phosphate buffer. The 50-μL reaction was incubated at 37°C for 1 h and then stopped by the addition of 200 μL 2-amino-2-methylpropanol (100 mM, pH 10) (Sigma-Aldrich). Endpoint fluorescence (360 nm, 450 nm) was taken by a Synergy Neo2 microplate reader (BioTek), measured in relative fluorescence units (RFU). For each sample, the identical procedure was concurrently performed using MUG (Toronto Research Chemicals), an uncharged substrate whose hydrolysis is independent of HexA but liberates the same MU fluorophore as MUGS.[3] The RFU value of MUGS was divided by that of MUG, becoming a unitless value. Because MUG hydrolysis is proportional to the total protein amount, irrespective of HexA quantity/activity, normalizing MUGS to MUG helps control for differences in protein quantity between samples despite 5 μg lysate intended across all samples.[3] Accordingly, true biological differences in HexA function are better detected without being obfuscated by experimental inconsistencies in HexA quantity. This normalized level of MUGS hydrolysis was then multiplied by 100 to produce the final unscaled HexA function score that we report to quantify HexA activity for each sample.

Fluorescent staining and analysis

LysoTracker staining

A total of 200,000 cells were seeded per well in a 12-well plate and cultured overnight. Cells were then stained with LysoTracker red DND-99 (Thermo Fisher Scientific) diluted to 1 μM in warmed media at 37°C in the dark for 1 h. Nuclei were counterstained with 10 μg/mL Hoescht 33342 for 15 min followed by PBS washing. Fluorescence intensity (577 nm, 590 nm) was read using a Synergy Neo2 plate reader (Agilent), with LysoTracker intensity normalized to that of Hoescht. Visual assessment of stained lysosomes was done with a Lionheart FX automated microscope (Agilent) using red fluorescent protein and DAPI filter sets.

Nile red staining

Cells were prepared as described for LysoTracker staining. Nile Red (Thermo Fisher Scientific) was reconstituted in DMSO and diluted to 1 μM in warmed media to stain cells for 15 min at 37°C in the dark. Cells were fixed with 4% paraformaldehyde for 15 min, followed by nuclear staining with Hoescht in the manner described above. Yellow-gold fluorescence was measured to target neutral lipid content (i.e., cytoplasmic lipid droplets [515 nm, 585 nm]).[51] Using Prolong Gold Antifade Mountant (Thermo Fisher Scientific), cells were mounted onto glass slides and then imaged using a spinning disk confocal microscope (Quorum Technologies) with an EM-CCD C9100-13 camera (Hamamatsu).

GM2 immunofluorescent staining

Cells were seeded in a 12-well plate on glass coverslips coated with Gibco collagen I and rat tail (Fisher Scientific) and grown overnight to ∼80% confluency. After 4% paraformaldehyde fixation for 15 min, cells were permeabilized using 0.1% Triton X-100 for 15 min and then blocked in 3% BSA for 1 h, all with PBS diluent at room temperature. PBS washes took place between steps. Mouse monoclonal anti-GM2 (MK1-16, TCI America) was then incubated at room temperature for 1 h (1:800 dilution). The secondary probe was done using CoraLite488-conjugated goat anti-mouse

immunoglobulin G (H + L) (Proteintech Group) for 1 h at room temperature (1:1,000 dilution). DAPI was used to stain nuclei for 10 min, followed by coverslip mounting onto glass slides using ProLong Glass Antifade Mountant (Thermo Fisher Scientific) and sealing with clear nail polish. Images were captured by spinning disk confocal microscopy as above.

Software use and statistical tests

DNA sequence visualization and manipulation were done in SnapGene (Dotmatics). The annotated *HEXA* genomic sequence was retrieved from the NCBI database (GenBank: NC_000015; Gene ID: 3073). PDB Mol* was used to generate 3D images of HexA.[52] Figures were created using BioRender, and statistical tests were performed by R version 4.2.2. Error bars on graphs indicate SDs. The following significance levels are noted: $*p < 0.05$; $**p < 0.01$; $***p < 0.001$.

DATA AND CODE AVAILABILITY

Data are available by request from the corresponding author.

ACKNOWLEDGMENTS

This work was made possible by funding from the Blu Genes Foundation, the Canadian Institutes of Health Research, and the SickKids Research Training Centre. We are grateful to Michael Tropak for guidance on the cellular assays, and we thank all of our colleagues in the Cohn and Ivakine labs for their support.

AUTHOR CONTRIBUTIONS

Conceptualization, J.E.H. and E.A.I. Methodology, J.E.H., R.A.B., A.M., and E.A.I. Validation, J.E.H. and E.A.I. Formal analysis, J.E.H. and E.A.I. Investigation, J.E.H., L.E., R.A.B., and G.F. Resources, E.A.I. Data curation, J.E.H. Writing – original draft, J.E.H. Writing – review & editing, G.F., W.S.C., E.A.I., and J.E.H. Visualization, J.E.H. Supervision, E.A.I. Project administration, E.A.I. Funding acquisition, J.E.H. and E.A.I.

DECLARATION OF INTERESTS

The authors declare no competing interests.

SUPPLEMENTAL INFORMATION

Supplemental information can be found online at https://doi.org/10.1016/j.omtn.2024.102401.

REFERENCES

1. Tropak, M.B., Yonekawa, S., Karumuthil-Melethil, S., Thompson, P., Wakarchuk, W., Gray, S.J., Walia, J.S., Mark, B.L., and Mahuran, D. (2016). Construction of a hybrid β-hexosaminidase subunit capable of forming stable homodimers that hydrolyze GM2 ganglioside in vivo. Mol. Ther. Methods Clin. Dev. *3*, 15057.
2. O'dowd, B.F., Cumming, D.A., Mahuran, D., and Gravel, R.A. (1988). Oligosaccharide structure and amino acid sequence of the major glycopeptides of mature human beta-hexosaminidase. Biochemistry *27*, 5216–5226.
3. Sharma, R., Deng, H., Leung, A., and Mahuran, D. (2001). Identification of the 6-Sulfate Binding Site Unique to α-Subunit-Containing Isozymes of Human β-Hexosaminidase. Biochemistry *40*, 5440–5446.
4. Solovyeva, V.V., Shaimardanova, A.A., Chulpanova, D.S., Kitaeva, K.V., Chakrabarti, L., and Rizvanov, A.A. (2018). New approaches to Tay-Sachs disease therapy. Front. Physiol. *9*, 1663. https://doi.org/10.3389/fphys.2018.01663.
5. Mahuran, D.J. (1998). The GM2 activator protein, its roles as a co-factor in GM2 hydrolysis and as a general glycolipid transport protein. Biochim. Biophys. Acta *1393*, 1–18.
6. Leal, A.F., Benincore-Flórez, E., Solano-Galarza, D., Jaramillo, R.G.G., Echeverri-Peña, O.Y., Suarez, D.A., Alméciga-Díaz, C.J., and Espejo-Mojica, A.J. (2020). GM2 Gangliosidoses: Clinical Features, Pathophysiological Aspects, and Current Therapies. Int. J. Mol. Sci. *21*, 1–27.
7. Toro, C., Zainab, M., and Tifft, C.J. (2021). The GM2 gangliosidoses: Unlocking the mysteries of pathogenesis and treatment. Neurosci. Lett. *764*, 136195.
8. Ibrahim, D.M.A., Ali, O.S.M., Nasr, H., Fateen, E., and AbdelAleem, A. (2023). Biochemical and mutational analyses of HEXA in a cohort of Egyptian patients with infantile Tay-Sachs disease. Expansion of the mutation spectrum. Orphanet J. Rare Dis. *18*, 52–59.
9. Giraud, C., Dussau, J., Azouguene, E., Feillet, F., Puech, J.P., and Caillaud, C. (2010). Rapid identification of HEXA mutations in Tay-Sachs patients. Biochem. Biophys. Res. Commun. *392*, 599–602.
10. Akli, S., Chelly, J., Kahn, A., and Poenaru, L. (1993). A null allele frequent in non-Jewish Tay-Sachs patients. Hum. Genet. *90*, 614–620.
11. Frisch, A., Colombo, R., Michaelovsky, E., Karpati, M., Goldman, B., and Peleg, L. (2004). Origin and spread of the 1278insTATC mutation causing Tay-Sachs disease in Ashkenazi Jews: Genetic drift as a robust and parsimonious hypothesis. Hum. Genet. *114*, 366–376.
12. Park, N.J., Morgan, C., Sharma, R., Li, Y., Lobo, R.M., Redman, J.B., Salazar, D., Sun, W., Neidich, J.A., and Strom, C.M. (2010). Improving accuracy of tay sachs carrier screening of the non-jewish population: Analysis of 34 carriers and six late-onset patients with hexa enzyme and dna sequence analysis. Pediatr. Res. *67*, 217–220.
13. Rajavel, K.S., and Neufeld, E.F. (2001). Nonsense-Mediated Decay of Human HEXA mRNA. Mol. Cell Biol. *21*, 5512–5519.
14. Jarnes Utz, J.R., Kim, S., King, K., Ziegler, R., Schema, L., Redtree, E.S., and Whitley, C.B. (2017). Infantile Gangliosidoses: Mapping a Timeline of Clinical Changes. Mol. Genet. Metabol. *121*, 170–179.
15. Masingue, M., Dufour, L., Lenglet, T., Saleille, L., Goizet, C., Ayrignac, X., Ory-Magne, F., Barth, M., Lamari, F., Mandia, D., et al. (2020). Natural History of Adult Patients with GM2 Gangliosidosis. Ann. Neurol. *87*, 609–617.
16. MacQueen, G.M., Rosebush, P.I., and Mazurek, M.F. (1998). Neuropsychiatric aspects of the adult variant of Tay-Sachs disease. J. Neuropsychiatry Clin. Neurosci. *10*, 10–19.
17. Leinekugel, P., Michel, S., Conzelmann, E., and Sandhoff, K. (1992). Quantitative correlation between the residual activity of β-hexosaminidase A and arylsulfatase A and the severity of the resulting lysosomal storage disease. Hum. Genet. *88*, 513–523.
18. Picache, J.A., Zheng, W., and Chen, C.Z. (2022). Therapeutic Strategies For Tay-Sachs Disease. Front. Pharmacol. *13*, 906647.
19. Marrone, L., Marchi, P.M., and Azzouz, M. (2022). Circumventing the packaging limit of AAV-mediated gene replacement therapy for neurological disorders. Expet Opin. Biol. Ther. *22*, 1163–1176. https://doi.org/10.1080/14712598.2022.2012148.
20. Iyer, S., Suresh, S., Guo, D., Daman, K., Chen, J.C.J., Liu, P., Zieger, M., Luk, K., Roscoe, B.P., Mueller, C., et al. (2019). Precise therapeutic gene correction by a simple nuclease-induced double-stranded break. Nature *568*, 561–565.
21. Erkut, E., and Yokota, T. (2022). CRISPR Therapeutics for Duchenne Muscular Dystrophy. Int. J. Mol. Sci. *23*, 1832.
22. Happi Mbakam, C., Lamothe, G., Tremblay, G., and Tremblay, J.P. (2022). CRISPR-Cas9 Gene Therapy for Duchenne Muscular Dystrophy. Neurotherapeutics *19*, 931–941.
23. Agrawal, P., Harish, V., Mohd, S., Singh, S.K., Tewari, D., Tatiparthi, R., Harshita, Vishwas, S., Sutrapu, S., Dua, K., and Gulati, M. (2023). Role of CRISPR/Cas9 in the treatment of Duchenne muscular dystrophy and its delivery strategies. Life Sci. *330*, 122003.
24. Erwood, S., Brewer, R.A., Bily, T.M.I., Maino, E., Zhou, L., Cohn, R.D., and Ivakine, E.A. (2019). Modeling Niemann-Pick disease type C in a human haploid cell line allows for patient variant characterization and clinical interpretation. Genome Res. *29*, 2010–2019.
25. Barritt, A.W., Anderson, S.J., Leigh, P.N., and Ridha, B.H. (2017). Late-onset Tay–Sachs disease. Practical Neurol. *17*, 396–399.
26. Navon, R., Kolodny, E.H., Mitsumoto, H., Thomas, G.H., and Proia, R.L. (1990). Ashkenazi-Jewish and non-Jewish adult GM2 gangliosidosis patients share a common genetic defect. Am. J. Hum. Genet. *46*, 817–821.

27. Fernandes, M.J., Hechtman, P., Boulay, B., and Kaplan, F. (1997). A Chronic GM2 Gangliosidosis Variant with a HEXA Splicing Defect: Quantitation of HEXA mRNAs in Normal and Mutant Fibroblasts. Eur. J. Hum. Genet. *5*, 129–136.

28. Parnes, S., Karpati, G., Carpenter, S., Kin, N.M., Wolfe, L.S., and Suranyi, L. (1985). Hexosaminidase-A Deficiency Presenting as Atypical Juvenile-onset Spinal Muscular Atrophy. Arch. Neurol. *42*, 1176–1180.

29. Levit, A., Nutman, D., Osher, E., Kamhi, E., and Navon, R. (2010). Two novel exonic point mutations in HEXA identified in a juvenile Tay-Sachs patient: role of alternative splicing and nonsense-mediated mRNA decay. Mol. Genet. Metabol. *100*, 176–183.

30. Maegawa, G.H.B., Tropak, M., Buttner, J., Stockley, T., Kok, F., Clarke, J.T.R., and Mahuran, D.J. (2007). Pyrimethamine as a potential pharmacological chaperone for late-onset forms of GM2 gangliosidosis. J. Biol. Chem. *282*, 9150–9161.

31. Georgiou, T., Christopoulos, G., Anastasiadou, V., Hadjiloizou, S., Cregeen, D., Jackson, M., Mavrikiou, G., Kleanthous, M., and Drousiotou, A. (2014). The first family with Tay-Sachs disease in Cyprus: Genetic analysis reveals a nonsense (c.78G>A) and a silent (c.1305C>T) mutation and allows preimplantation genetic diagnosis. Meta gene *2*, 200–205.

32. Grajcarek, J., Monlong, J., Nishinaka-Arai, Y., Nakamura, M., Nagai, M., Matsuo, S., Lougheed, D., Sakurai, H., Saito, M.K., Bourque, G., and Woltjen, K. (2019). Genome-wide microhomologies enable precise template-free editing of biologically relevant deletion mutations. Nat. Commun. *10*, 4856–4913.

33. Walton, R.T., Christie, K.A., Whittaker, M.N., and Kleinstiver, B.P. (2020). Unconstrained genome targeting with near-PAMless engineered CRISPR-Cas9 variants. Science *368*, 290–296.

34. Lemieux, M.J., Mark, B.L., Cherney, M.M., Withers, S.G., Mahuran, D.J., and James, M.N.G. (2006). Crystallographic Structure of Human β-Hexosaminidase A: Interpretation of Tay-Sachs Mutations and Loss of GM2 Ganglioside Hydrolysis. J. Mol. Biol. *359*, 913–929.

35. Dersh, D., Iwamoto, Y., and Argon, Y. (2016). Tay–Sachs disease mutations in HEXA target the α chain of hexosaminidase A to endoplasmic reticulum–associated degradation. Mol. Biol. Cell *27*, 3813–3827.

36. Takashima, S., Shinkuma, S., Fujita, Y., Nomura, T., Ujiie, H., Natsuga, K., Iwata, H., Nakamura, H., Vorobyev, A., Abe, R., and Shimizu, H. (2019). Efficient Gene Reframing Therapy for Recessive Dystrophic Epidermolysis Bullosa with CRISPR/Cas9. J. Invest. Dermatol. *139*, 1711–1721.e4.

37. Fisher, G., Mackels, L., Markati, T., Sarkozy, A., Ochala, J., Jungbluth, H., Ramdas, S., and Servais, L. (2022). Early clinical and pre-clinical therapy development in Nemaline myopathy. Expert Opin. Ther. Targets *26*, 853–867.

38. Takeda, S., Clemens, P.R., and Hoffman, E.P. (2021). Exon-Skipping in Duchenne Muscular Dystrophy. J. Neuromuscul. Dis. *8*, S343–S358.

39. Lalonde, S., Stone, O.A., Lessard, S., Lavertu, A., Desjardins, J., Beaudoin, M., Rivas, M., Stainier, D.Y.R., and Lettre, G. (2017). Frameshift indels introduced by genome editing can lead to in-frame exon skipping. PLoS One *12*, e0178700.

40. Turczynski, S., Titeux, M., Pironon, N., and Hovnanian, A. (2012). Antisense-mediated exon skipping to reframe transcripts. Methods Mol. Biol. *867*, 221–238.

41. Brambati, A., Barry, R.M., and Sfeir, A. (2020). DNA polymerase theta (Polθ) - an error-prone polymerase necessary for genome stability. Curr. Opin. Genet. Dev. *60*, 119–126.

42. Pasquini, G., Kempe, A., Karl, M.O., Stieger, K., and Busskamp, V. (2019). Transcriptomic assessing and guiding DSB repair pathway activity towards precise genomic engineering of post-mitotic neurons. Invest. Ophthalmol. Vis. Sci. *60*.

43. Guidotti, J., Akli, S., Castelnau-Ptakhine, L., Kahn, A., and Poenaru, L. (1998). Retrovirus-mediated enzymatic correction of Tay-Sachs defect in transduced and non-transduced cells. Hum. Mol. Genet. *7*, 831–838.

44. Anzalone, A.V., Randolph, P.B., Davis, J.R., Sousa, A.A., Koblan, L.W., Levy, J.M., Chen, P.J., Wilson, C., Newby, G.A., Raguram, A., and Liu, D.R. (2019). Search-and-replace genome editing without double-strand breaks or donor DNA. Nature *576*, 149–157.

45. Labun, K., Montague, T.G., Krause, M., Torres Cleuren, Y.N., Tjeldnes, H., and Valen, E. (2019). CHOPCHOP v3: Expanding the CRISPR web toolbox beyond genome editing. Nucleic Acids Res. *47*, W171–W174.

46. Varshney, G.K., Carrington, B., Pei, W., Bishop, K., Chen, Z., Fan, C., Xu, L., Jones, M., LaFave, M.C., Ledin, J., et al. (2016). A high-throughput functional genomics workflow based on CRISPR/Cas9-mediated targeted mutagenesis in zebrafish. Nat. Protoc. *11*, 2357–2375.

47. Doman, J.L., Sousa, A.A., Randolph, P.B., Chen, P.J., and Liu, D.R. (2022). Designing and executing prime editing experiments in mammalian cells. Nat. Protoc. *17*, 2431–2468.

48. Hwang, G.H., Jeong, Y.K., Habib, O., Hong, S.A., Lim, K., Kim, J.S., and Bae, S. (2021). PE-Designer and PE-analyzer: Web-based design and analysis tools for CRISPR prime editing. Nucleic Acids Res. *49*, W499–W504.

49. Nelson, J.W., Randolph, P.B., Shen, S.P., Everette, K.A., Chen, P.J., Anzalone, A.V., An, M., Newby, G.A., Chen, J.C., Hsu, A., and Liu, D.R. (2021). Engineered pegRNAs improve prime editing efficiency. Nat. Biotechnol. *40*, 402–410.

50. Conant, D., Hsiau, T., Rossi, N., Oki, J., Maures, T., Waite, K., Yang, J., Joshi, S., Kelso, R., Holden, K., et al. (2022). Inference of CRISPR Edits from Sanger Trace Data. Cris. J. *5*, 123–130.

51. Greenspan, P., Mayer, E.P., and Fowler, S.D. (1985). Nile red: A selective fluorescent stain for intracellular lipid droplets. J. Cell Biol. *100*, 965–973.

52. Sehnal, D., Bittrich, S., Deshpande, M., Svobodová, R., Berka, K., Bazgier, V., Velankar, S., Burley, S.K., Koča, J., and Rose, A.S. (2021). Mol* Viewer: modern web app for 3D visualization and analysis of large biomolecular structures. Nucleic Acids Res. *49*, W431–W437.